quaternary

MDPI

Article

Sedimentological and Ecological Controls on Heavy Metal Distributions in a Mediterranean Shallow Coastal Lake (Lake Ganzirri, Italy)

Roberta Somma [1,*], Mohammadali Ghanadzadeh Yazdi [1], Majed Abyat [1], Raymart Keiser Manguerra [2], Salvatore Zaccaro [2], Antonella Cinzia Marra [1] and Salvatore Giacobbe [3]

[1] Dipartimento di Scienze Matematiche e Informatiche, Scienze Fisiche e Scienze della Terra, Università degli Studi di Messina, Viale F. Stagno d'Alcontres, 31, 98166 Messina, Italy
[2] Ph3 Engineering S.r.l., Caio Duilio, 2, 98123 Messina, Italy; kmanguerra@ph3srl.it (R.K.M.); szaccaro@ph3srl.it (S.Z.)
[3] Dipartimento di Scienze Chimiche, Biologiche, Farmaceutiche ed Ambientali, Università degli Studi di Messina, Viale Ferdinando Stagno d'Alcontres, 31, 98166 Messina, Italy
* Correspondence: rsomma@unime.it

Abstract

Coastal lakes are highly vulnerable transitional systems in which sedimentological processes and benthic ecological conditions jointly control contaminant accumulation and preservation, particularly in densely urbanized settings. A robust understanding of the physical and ecological characteristics of bottom sediments is therefore essential for the correct interpretation of contaminant distributions, including those of potentially toxic metals. In this study, an integrated sedimentological–ecological approach was applied to Lake Ganzirri, a Mediterranean shallow coastal lake located in northeastern Sicily (Italy), where recent investigations have identified localized heavy metal anomalies in surface sediments. Sediment texture, petrographic and mineralogical composition, malacofaunal assemblages, and lake-floor morpho-bathymetry were systematically analysed using grain-size statistics, faunistic determinations, GIS-based spatial mapping, and bivariate and multivariate statistical methods. The modern lake bottom is dominated by bioclastic quartzo-lithic sands with low fine-grained fractions and variable but locally high contents of calcareous skeletal remains, mainly derived from molluscs. Sediments are texturally heterogeneous, consisting predominantly of coarse-grained sands with lenses of very coarse sand, along with gravel and subordinate medium-grained sands. Both sedimentological features and malacofaunal death assemblages indicate deposition under open-lagoon conditions characterized by brackish waters and relatively high hydrodynamic energy. Spatial comparison between sedimentological–ecological parameters and previously published heavy metal distributions reveals no significant correlations with metal hotspots. The generally low metal concentrations, mostly below regulatory threshold values, are interpreted as being favoured by the high permeability and mobility of coarse sediments and by energetic hydrodynamic conditions limiting fine-particle accumulation. Overall, the integration of sedimentological and ecological data provides a robust framework for interpreting contaminant patterns and offers valuable insights for the environmental assessment and management of vulnerable coastal lake systems, as well as for the understanding of modern lagoonal sedimentary processes.

Keywords: modern coastal lake systems; quaternary geology; morpho-bathymetry; sedimentology; mineralogy; ecology; malacofauna; GIS maps; bivariate and multivariate statistics

Check for updates

Academic Editor: James B. Innes

Received: 13 December 2025
Revised: 20 January 2026
Accepted: 21 January 2026
Published: 23 January 2026

Copyright: © 2026 by the authors. Licensee MDPI, Basel, Switzerland. This article is an open access article distributed under the terms and conditions of the Creative Commons Attribution (CC BY) license.

1. Introduction

Transitional waters, including estuaries and coastal lake systems, represent biotopes of primary importance because of their regulatory role in exchanges between continental and marine environments. Moreover, they support high primary and secondary production, being characterized by marked ecological gradients and high levels of biodiversity.

However, transitional environments are intrinsically vulnerable due to omnifarious pressures of both natural and anthropogenic origin, such as climate change, subsidence, coastal erosion, pollution, mass tourism, coastal urbanization, and resource overexploitation [1].

Among the several typologies of transitional environments, small and shallow brackish coastal lakes are severely threatened due to their limited broadness and resilience, especially when located within or close to anthropized lands [1,2]. In such cases, brackish coastal lakes are mostly heterogeneous and complex systems, with several local peculiarities spread out along strong marine–continental gradients. Consequently, investigations aimed at characterizing their state of health or at indicating contamination processes need to be supported by adequate knowledge of the physical environment, including the primary characterization of bottom sediments (texture, composition, and malacofauna). This requirement is particularly stringent in the case of mineral contaminants, such as heavy metals, whose concentration may be strongly correlated with fine sediments, as well as with organic matter and clay minerals. Thus, knowledge of such background is essential at any specific site for the proper assessment of its ecological risk or the planning of effective remediation interventions. Moreover, distinguishing natural and anthropogenic sources for heavy metals may play an important role in environmental protection and policies (see [3,4] and references therein). Heavy metal hotspots near anthropogenic sources (anthropogenic channels, discharge pipes, etc.) and associated with decreasing gradients towards the most distal areas may be suspected sites to be investigated with priority. Concentrations comparable to those of pre-industrial backgrounds (namely, element concentrations naturally present in the environmental matrix) may be indicative of a natural source where metal accumulation in aquatic environments may derive from weathering and leaching of rocks containing these elements. Indeed, metals can be dissolved in water and removed through sorption on solid particles of suspended matter or because of precipitation and bonding in the mineral crystalline lattice [5]. Notwithstanding, such elements may be released again in the environment because of changing environmental factors and absorbed by the bioavailable sediment fractions (see [5] and references therein).

In this regard, an appropriate case study of sedimentological and ecological investigations is provided by Lake Ganzirri (hereafter LG) (Messina, NE Sicily, Italy), being an example of a brackish environment in the Mediterranean area [6–9] that, like other Italian brackish lagoons (Lesina, Varano, Venice, and Orbetello lagoons), is subjected to significant anthropogenic pressures (vehicular traffic, mass tourism, and coastal urbanization), despite the lake being subject to different levels of protection. Notwithstanding its recognized naturalistic value, coupled with the heritage of ancient practices of environmentally friendly exploitation of natural resources [10], only scattered data were reported in the past on the environmental status of LG. More recently, studies on the environmental and ecological background were published [11–14]. Among them, an investigation of potential contaminant metals put in evidence some local geochemical hotspots in the bottom sediments [15]. These anomalies need to be better interpreted in the context of the morpho-bathymetric, geological, sedimentological, mineralogical, and ecological features of the basin.

With this in mind, the present research on LG is devoted to (i) the morpho-bathymetric and geological characterization of the lake bottom, (ii) the textural and compositional

characterization of the actual bottom bed (including determination of the malacofauna), and (iii) the description of possible hotspots in the spatial distribution of the main textural and bioclast features for comparison with chemical hotspots of heavy metals and other metals known in the literature [15]. This multi-disciplinary approach based on the investigation of the relationships between the dynamics of sediments, structural controls, ecological distribution patterns, and background conditions of heavy metals could be a useful method for characterizing the state of health of vulnerable coastal lake systems and better managing them. Moreover, the research results could also contribute by providing new insights into modern coastal lagoon systems.

2. Sedimentary Processes in Lakes

Repeated transgressive–regressive lake-level cycles linked to lake-level fluctuations (driven by climate or tectonics) may be recorded in the stratigraphic successions of coastal lake systems [16]. Transgressive successions record landward shoreline retrogradation in response to relative lake-level rise and/or diminished sediment supply. They are usually fining-upward and may show alluvial deposits evolving upwards to shoreline sands and, finally, to offshore muds characterized by increasing organic matter [16–20]. Conversely, regressive successions reflect basin-ward shoreline progradation driven by relative lake-level fall and/or enhanced sediment supply. They are usually coarsening-upward and may show offshore muds evolving upwards to deltaic sand and, finally, to fluvial deposits [16–20]. In such cases, abrupt heteropic facies transitions may be present, being commonly linked to rapid lake-level fluctuations [16–20]. Finally, paleo-seasonal and paleo-climatic forcings may be recorded by rhythmic laminations [16].

In such depositional systems, transport and deposition may be influenced by several factors [16–20]. Alternate stratification and convective processes in the water column may lead to differential sedimentation, where fine-grained sediments (silt and clay) settle more slowly under low-energy conditions, while coarse-grained sediments (sand and gravel) settle during more energetic periods [16,17]. The lake-basin centre may be characterized by the presence of muds; turbidites; or, in arid climates, evaporites [16–20]. In contrast, the lake margins show the occurrence of fluvial and deltaic clastic sediments laterally interbedded with those present in the basin centre [16]. Among the main physical processes ruling transport and deposition, kinetic energy may be the most relevant, since the flow velocity strongly influences the grain-size distribution [17]. High-energy conditions may transport larger grains, while low-energy conditions allow finer particles to settle [18]. Rivers or streams that feed into shallow lakes bring sediments with varying grain sizes, whose differential deposition is usually ruled by the energy of the flows entering the lake. This depends on the distance at which the water velocity drops below the critical settling velocity for a given grain size. Similar effects may be due to tidal currents flowing in the coastal channels connecting lakes to the sea/ocean. Decomposition of organic matter by microbes may release nutrients into the water, influencing the formation of dark sediments rich in organic matter.

High-energy conditions usually prevail in small and shallow lakes. Deposition is controlled by wave action, fluctuations in water levels, or wind, mostly favouring the deposition of coarse-grained sediments [16]. Clastic deposits are generally characterized by well-sorted sediments with low contents in fine fractions. The sand distribution is mainly influenced by a complex balance of interacting sediment input, hydraulic dynamics, bottom morphology, and biological factors. In the more exposed, high-energy zones, such as those along the lake margins or near lake mouths, crests, or mounds, coarser and well-sorted sands usually prevail. Submerged vegetation, such as seagrasses and floating algae contrasting wave motion and currents, may retain finer sediments at the edges of meadows.

Notwithstanding, low-energy conditions may also occur in shallow lakes, particularly offshore in the most distal areas away from the shoreline.

Low-energy conditions usually prevail in deep lakes. Deposition is primarily controlled by slow settling from suspension. Fine-grained sediments are typically transported through the water column and deposited more evenly [16,17]. In such areas, the deposition of fine sediments usually prevails. Depressed areas tend to accumulate poorly sorted fine sediments, but turbiditic flows may also occur. In coastal lakes, exceptional events such as sea storms or tsunamis may also strongly modify the original depositional system [21].

Textural sedimentological parameters and malacofauna features allow for diagnosis of both modern and past depositional environments, reflecting transport modalities and energy conditions of the transporting medium [20].

3. Geological and Ecological Background

Lake Ganzirri is located on the Ionian coast of the Cape Peloro peninsula, on the NE edge of the Peloritani chain (Figure 1a) [11]. The latter, belonging to the Calabria–Peloritani Arc structure, crops out from the "Taormina–Sant'Agata di Militello tectonic line" in the SW to Cape Peloro in the NE (Figure 1a) [22]. The chain is formed by five main tectonic units [22] composed of Variscan crystalline basements and their Meso-Cenozoic cover [22–25]. During the Miocene, a post-orogenic uplift involved the chain, producing significant volumes of siliciclastic deposits whose source rocks mostly derived from the Variscan crystalline rocks of the Calabria–Peloritani Arc [26]. The hills constituting the hinterland of the Cape Peloro peninsula are mainly composed of Variscan high-grade metamorphic rocks (Paleozoic gneiss and gneissic mica schists intruded by igneous rocks; Aspromonte Unit) covered by Miocene to middle Pleistocene sediments (Figure 1a–c). The modern coastal deposits [26], usually considered younger than 5.9 ka [27], are composed of sandy and gravelly sediments (~60 m thick) [26,28], mostly deriving from the re-elaboration of the middle Pleistocene siliciclastic deposits [29] present in the substrate and in the surrounding hilly areas (Figure 1d).

3.1. Study Area

Lake Ganzirri stretches along an ENE–WSW direction and is parallel to the Sicilian Ionian coast of the northern end of the Strait of Messina. The ENE–WSW elongated shape is interpreted as being due to the morpho-tectonic control of the ENE–WSW-trending capable normal fault system of Scilla–Ganzirri [30–32], which is responsible for the orientation of the Ionian coast in this part of the Strait of Messina, as well as for the development of the ENE–WSW-trending Ganzirri graben hosting the lake (Figure 1d) [11].

The lake (long axis: 1668 m; short axis: 266 m) covers an area of ~312,076 m^2 and reaches a maximum depth of 7 m in its westernmost portion. Two sub-elliptically shaped sub-basins separated by a narrow zone can be distinguished. The easternmost one, known as Madonna di Trapani (hereafter ESB), is notably smaller and shallower than the westernmost sub-basin (hereafter WSB). Because of its shallow waters, most of the clam farming activities are concentrated here.

The lake is located at a minimum distance of 125 m from the Ionian Sea, to which it is connected via two artificial canals named "Catuso" (n. 1 in Figure 1d) and "Due Torri" (n. 2 in Figure 1d); however, only the latter guarantees a regular and significant water exchange with the sea. A third canal named "Margi" connects LG with the nearby Lake Faro, realizing a further indirect but constant connection with the sea [11].

3.2. Previous Studies on the Late Holocene Environmental Conditions and Stratigraphic Features

During the Late Holocene, three distinct stages characterized the evolution of the lagoon of Cape Peloro. During prehistoric times, in the Early Middle Bronze Age, LG

was interconnected with Lake Faro, as well as with the sea [33]. During the Late Bronze Age, the connections with the sea were progressively reduced, and about 2600 y BP, the lagoon became isolated from the sea [34,35]. At the end of the 18th century, human action interrupted this period of confinement by means of digging canals that newly connected the lagoon to the sea [34,35].

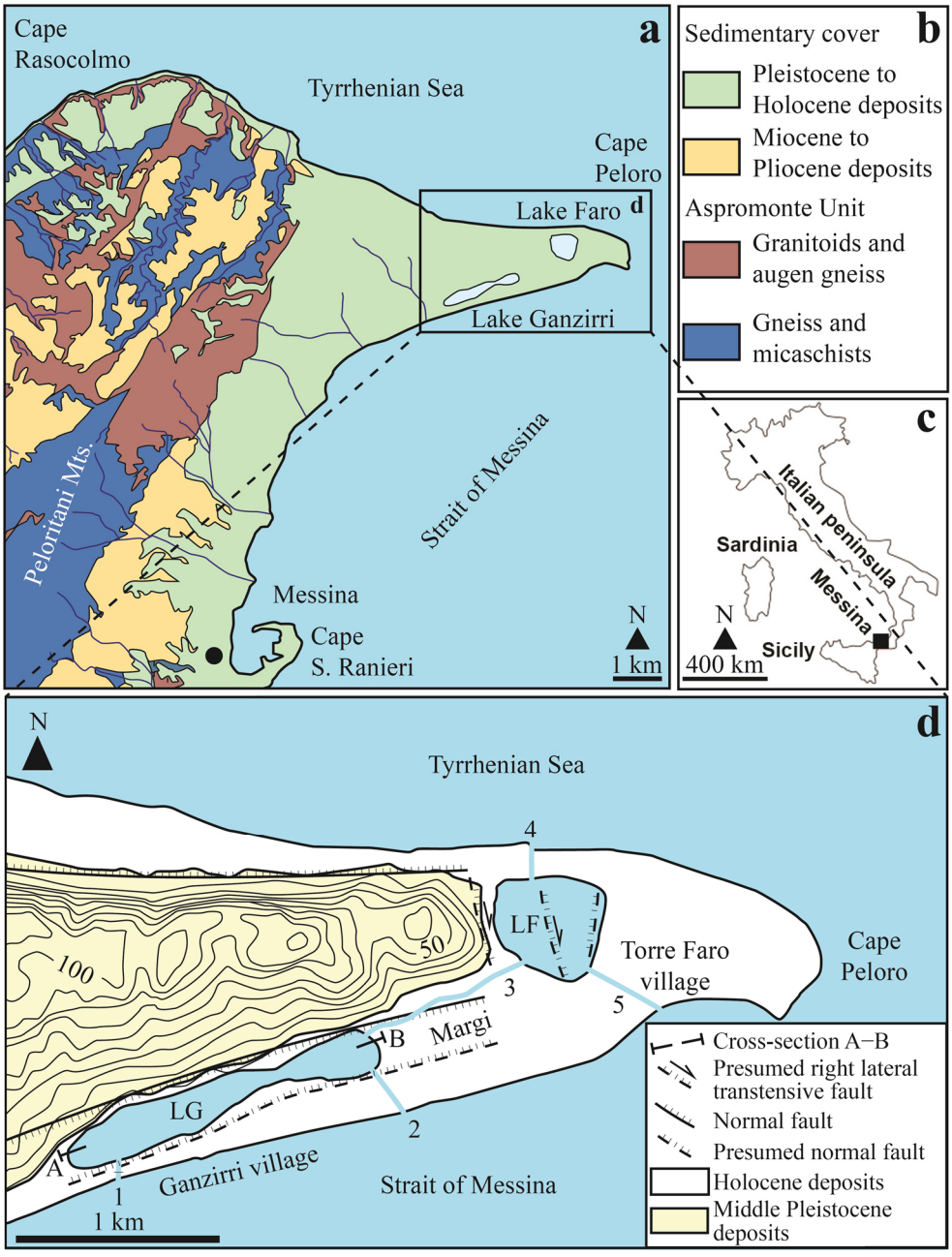


Figure 1. (**a**) Geological map of the NE end of the Peloritani Mountains (Messina, Italy). The rectangle shows the localization of the NE edge of Messina. (**b**) Legend of the geological map. (**c**) Localization of the study area. (**d**) Geological and structural map of the Cape Peloro peninsula. Isohypses are spaced at 10 m. Acronyms: LG, Lake Ganzirri; LF, Lake Faro. 1: Catuso Canal (currently closed); 2: Canal Due Torri; 3: Margi Canal; 4: degli Inglesi Canal; 5: Faro Canal.

The Late Holocene stratigraphic succession, dating back 3700 years, was analysed in LG for the first time only in recent times [34]. Three main facies associations (FAs) were identified (Figure 2). The oldest one (FA1, dating back to the Bronze Age) was made up of ~2 m thick massive or mostly massive sand with layers of organic matter and thin beds

of intact and fragmented molluscs (Figure 2). These characteristics indicated deposition within an open-lagoon environment. The intermediate facies association (FA2, dating back to the time interval ranging between 2600 y BP and 150 y BP) was the thickest one (~4.80 m). It was composed of silty sands thinly laminated and rich in organic matter and intercalated by two massive sandy beds (Figure 2). These characteristics indicated deposition within a confined lagoon. Finally, the youngest facies association (FA3, younger than 150 y BP) was the thinnest one (0.44 m). It was made up of massive medium sand rich in mollusc shells and fragments (Figure 2). These characteristics indicated deposition within a reconnected lagoon that occurred when, during the 18th century, the lake artificially retrieved its connection to the sea.

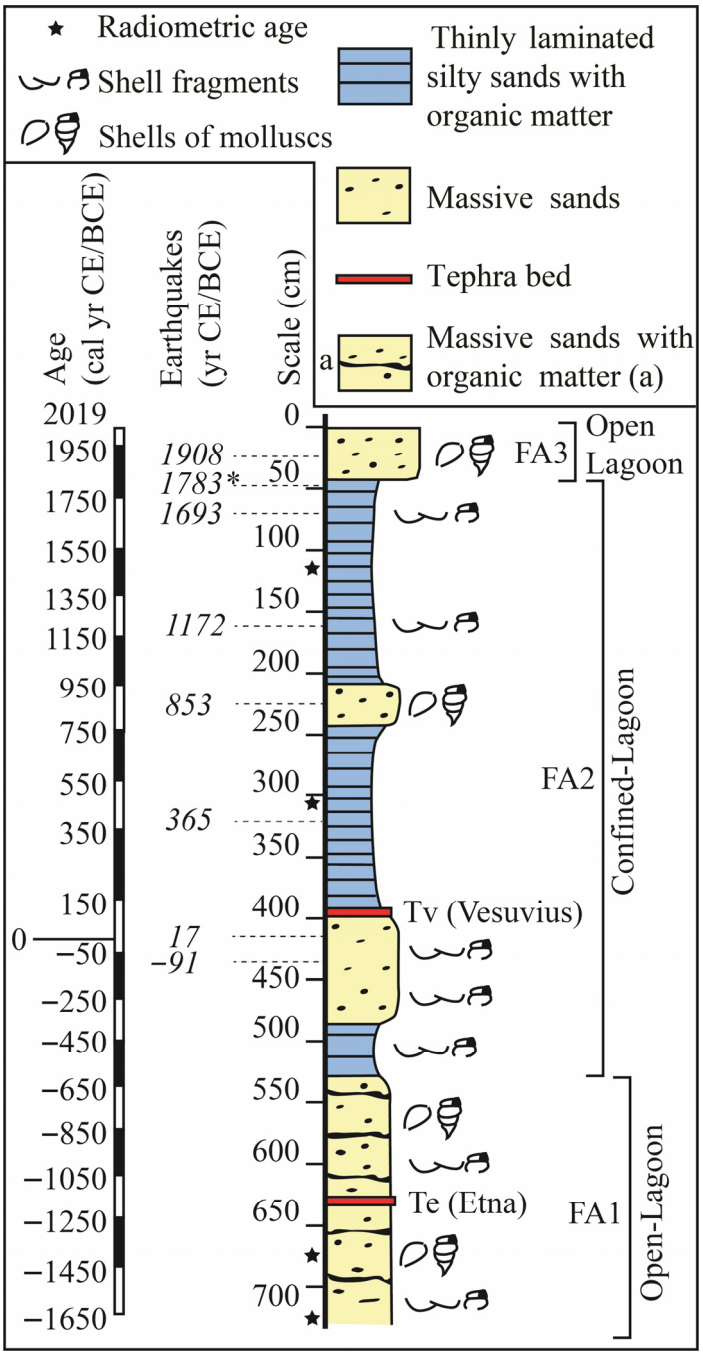


Figure 2. Stratigraphic record of Lake Ganzirri sediments (modified from [34]). The ages of the main earthquakes shaking the area are also reported. In particular, the 1783* earthquake was associated with a tsunami affecting LG.

3.3. Previous Studies on the Main Physical–Chemical Parameters and Ecological Constraints

Lake Ganzirri is classified as a mesotrophic–eutrophic basin [36] with anoxic/reduced conditions in the deepest waters. Among the most comprehensive studies, a multidisciplinary investigation characterized the seasonal hydrological parameters, the trophic conditions, and the microbial abundances and activities [37]. The trophic and microbial parameters, as well as the ecological status according to the synthetic trophic state index, were also investigated [38]. Moderate spatio–temporal oscillations affect LG waters due to the combined effects of marine tides, atmospheric pressure, and rainfall. The actual hydrodynamic regime is characterized by moderate energy levels [37,39]. Complete water renewal requires a minimum period of about 80 days [40]. The water temperature ranges seasonally from 26.93 °C to 29.43 °C, whereas the salinity varies seasonally from 14% to 35%. Except for sporadic and localized crises, dissolved oxygen saturation in the water is over the 100% level throughout the year, with higher values in spring and lower values in summer [37,39]. The water pH usually ranges from 8.05 to 8.50 [37,39]. The organic matter and carbonate contents in the sediments range from 0.1% to 28.1% and from 0.4% to 3.4%, respectively [41]. Low concentrations of heavy metals (lower than the threshold values indicated by Italian law) were detected in waters [42,43]. In recent times, very low concentrations of potentially toxic metals were also detected in clams [14]. Notwithstanding, evidence of plasticizers and bisphenols was found in edible clams, water, and sediments of LG [13]. In recent times, the fine distribution of potential mineral contaminants in the bioavailable fraction of the bottom sediments was investigated using different instrumental techniques [15]. This investigation pointed out that the metal concentrations were lower than the threshold values, except for some higher values of copper. Therefore, the distribution patterns of metals, as revealed by GIS maps, showed local geochemical anomalies (hotspots) related to higher concentrations for some elements.

4. Materials and Methods

4.1. Sediment Sampling and Morpho-Bathymetric Surveys

Soft sediments were collected from the bottom of LG at 47 stations as evenly distributed as possible throughout the lake. Twenty-three subsamples were also extracted for chemical analyses of metals [15]. Sediments were collected using a Van Veen grab with a 400 cm^2 sampling surface. The station depth was measured by means of a graduated bar. The number of surveyed bathymetric points reached a total of 68 stations, allowing for an upgrade of the only available bathymetric map dating back to 1952 [44]. Bathymetric and morphological surveys were integrated by means of scuba diving and remote sensing activities aimed at identifying anthropogenic structures such as artificial sandy mounds and piles of inert materials, as well as hard rock features.

4.2. Sedimentological Analyses

Sediments for grain-size analyses were pre-treated with H_2O_2 to reduce the organic matter content. Sediments were dried in an oven at T 80 °C and weighed when they reached a constant weight at T 20 °C. Sediments were also treated with a solution of sodium hexametaphosphate in distilled water to help disperse clay particles and prevent the formation of clay platelets.

Mechanical sieving was applied for coarse sediments (gravel and sand; grain size > 63 μm, 4 ϕ), whereas the laser diffraction technique (with sample dispersion in water) was used for defining the grain size of fine fractions (silt and clay; <63 μm, 4 ϕ). Both methods were applied in wet conditions.

The sieving was also aimed at separating coarse sediments in the different fractions (including the <63 μm particles used successively for the laser diffraction grain-size analyses) for further mineralogical and sedimentological characterizations.

Data were elaborated to obtain retained cumulative curves and classify sediments. The instrument used was a Retsch mechanical siever (model AS2, Haan, Germany). The pile of sieves was composed of 12 sieves (−4.2, −3.6, −3.2, −2.7, −2.2, −2.0, −1, 0, 1, 2, 3, and 4 ϕ). Statistical parameters were calculated using Folk and Ward's formula [45,46].

The laser diffraction technique was applied to obtain retained cumulative and frequency curves and classify the fine fraction [46–48]. The instrument used was a diffraction particle size analyser (Malvern Panalytical, Malvern, UK, model Mastersizer 2000) equipped with a dispersion unit (Hydro MU) used in wet conditions with distilled water. The measurable size range was between 0.02 and 2000 μm.

Lastly, the data used for reconstructing the total cumulative curve (i.e., from gravel to clay) were uploaded together to Microsoft Excel for Microsoft 365 (Microsoft Corp., Redmond, WA, USA), using spreadsheets elaborated by the authors, to obtain the retained cumulative curves of the total sediment samples, sediment classification, and textural statistical parameters.

4.3. Petrographic and Mineralogical Analyses

Mesoscale optical observations were accomplished and completed by petrographic and mineralogical analyses on thin sections of sands aggregated in epoxy. The instruments used were a stereomicroscope (Zeiss, Stereo Discovery model, Oberkochen, Germany) and a petrographic microscope (Axio Vision model, Zeiss, Oberkochen, Germany). Both microscopes were equipped with a Zeiss telecamera and a workstation for image analysis. Minor minerals were identified under a stereomicroscope, observing grain lustre, colour, habitus, and cleavage when observable.

4.4. Faunistic Determinations

The bioclastic contents of the five grain-size fractions corresponding to the 9.5 mm, 4.75 mm, 4 mm, 2 mm, and 1 mm sieves were quantitatively and qualitatively investigated. Faunistic determinations were carried out on bioclasts and shell remains, classified at the species level by using a stereomicroscope (Zeiss, Stereo Discovery model, Oberkochen, Germany). The nomenclature followed the World Register of Marine Species (WORMS) [48]. All species were scheduled in terms of presence/absence. The weight incidence of the most quantitatively relevant species was also evaluated.

4.5. Data Elaboration

QGIS software (QGIS desktop 3.28.10, version v30, Florence) was used for elaborating and visualizing 2D georeferenced maps related to the lake's morpho-bathymetric data, textural parameters, and bioclastic contents of the modern soft sediments [49]. Bivariate and multivariate analyses were also performed on the same data, using the PRIMER6 statistical software application [50] in the second case.

5. Results

5.1. Morpho-Bathymetric Map and Topographic Cross-Section

According to the depths recorded in the georeferenced stations (Figure 3a) and their interpolation in QGIS, a colour gradient map of LG's morpho-bathymetry was created (Figure 3b). Figure 3b shows that LG is characterized by two elongated and elliptically shaped sub-basins separated by a shallow and narrow zone (<1 m depth and 67 m width). The WSB, covering 2/3 of the lake surface (~224,754 m^2), is the major one (Figure 3b).

Bathymetry is variable, reaching a maximum depth of 6.5–7 m in the central sector (Figure 3b). In this area, a symmetric NNE–SSW-trending depression was observed. It is bounded by small cliffs that sharply intersect (about 70°) the ENE–WSW-trending northern and southern lake coasts (Figure 3b). The ESB, covering 1/3 of the lake surface (~87,322 m^2), is the minor one (Figure 3b). Its depth is about 1 m, except for a small depression of about 1.5 m depth close to the mouth of the Margi Canal to the east (Figure 3b).

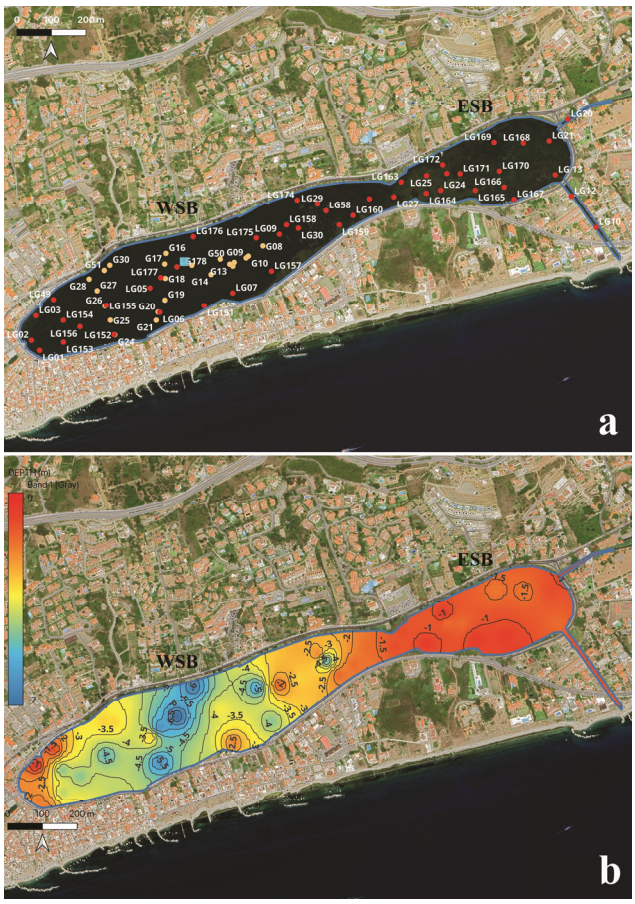


Figure 3. GIS maps of Lake Ganzirri. Acronyms: ESB, eastern sub-basin; WSB: western sub-basin. (**a**) Localization of the sixty-eight georeferenced stations used for reconstruction of the lake's bathymetry. Symbols: red circle, bottom soft sediment; yellow circle, unknown bedrock; light-blue square, drilling site [34]. (**b**) Morpho-bathymetric map of the lake bottom. The gradient colour scale (on the left) indicates areas with variable depths, from shallower (red) to deeper (blue) values. Isobaths are spaced at 0.5 m (the sign "-" corresponds to the minus sign).

An ENE–WSW topographic cross-section (Figure 4) was elaborated using the morpho-bathymetric data (Figure 3b).

In the WSB, six small cliffs with elevations of a few meters were identified (Figure 4). The westernmost cliffs dipped ESE-wards, opposite to the other cliffs dipping WNW-wards on the easternmost side of the same sub-basin.

On the western side of the ESB, the presence of a shallow barrier—evidence of an isthmus that, in past times, separated the two actual sub-basins—is recognizable (Figure 4). The upper Holocene beachrocks exposed out of the lake (near the lake's ENE edge and along the Cape Peloro peninsula and Ionian coast) presumably form and control the morpho-structure of the shallow and flat-lying platform of the ESB (Figure 4), analogously to what occurs on the platform of Lake Faro.

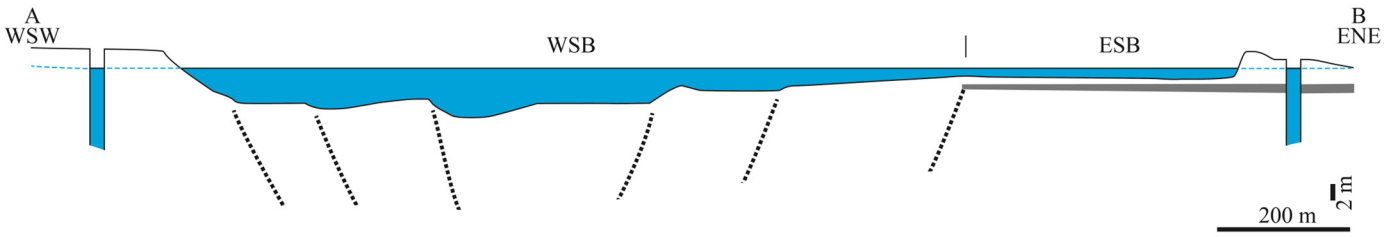


Figure 4. ENE–WSW-trending simplified topographic cross-section A-B of Lake Ganzirri. A presumed normal fault system (black dotted line) was reported in correspondence with the small cliffs observed on the bottom (see Discussion for further details). Holocene beachrocks were also reported (grey colour) in the ESB. The elevation is exaggerated with respect to the lake length because of a very low depth/length ratio (see different horizontal and vertical graphic scales). The cross-section orientation is indicated in Figure 1d.

The sampling of bottom soft sediments repeatedly failed at twenty-two stations, mostly distributed along three main alignments in the central sector of the WSB (Figure 3a). This anomaly has a plausible explanation in the presence of a hard substrate, whose nature is unknown. In fact, scuba diving surveys failed in recognizing the substrate typology due to the total absence of visibility underwater. Anthropogenic structures (tied to local clam farming practices) consisting of concrete blocks or waste materials were evident exclusively on the very shallow bottoms. A natural origin for the hard substrate appeared most realistic in the deeper bottom. In this context, the presence of siliciclastic sandy conglomerates of the Messina Formation (middle Pleistocene), being widely exposed in the surrounding areas, is highly probable.

5.2. Particle Size Analysis and Bivariate and Multivariate Statistics

Forty-six samples of sediments were analysed for grain-size characterization. Particle size analyses were also carried out on ten samples collected along the beaches of the Cape Peloro peninsula for comparative purposes. The Supplementary Materials contain the grain-size analysis data (Table S1), the grain-size cumulative curves (Figure S1a), and the gravel–sand–mud ternary plot (Figure S1).

5.2.1. Total Sediment Sample

The sediments were mainly represented by sand (~97.6%), with very low contents of silt (~1.8%) and clay (~0.6%) (Figure S1a,b). Only a few samples were classified as gravel (Figure S1a,b).

Sandy sediments were mostly coarse-grained and poorly sorted, with leptokurtic and nearly symmetrical distributions. Textural statistical parameters are reported in the Supplementary Materials (Figure S2).

The areal distributions of the textural statistical parameters (Figure 5) are described as follows.

- Mean (Mz) (Figures S2a and 5a): The widest outcrops were mostly formed by coarse-grained sand. Three lenses with very coarse-grained sand were distributed in the WSB. Small lenses of medium-grained sand were found in both sub-basins.
- Sorting (SD) (Figures S2b and 5b): The WSB's sediments were mostly very poorly sorted in the lake centre. A decreasing gradient from very poor sorting to poor and moderate sorting was observable from the lake centre WSW-wards and on the ENE edge. Analogously, the ESB sediments showed a WSW-wards decreasing gradient from the Margi Canal to the narrow zone between the two sub-basins. In the latter zone, sediments were poorly sorted.

- Kurtosis (Kg) (Figures S2c and 5c): The sediments were mostly leptokurtic. Lenses of strongly leptokurtic sediments prevailed on the western edge of the WSB; a few small-sized lenses were also present in the narrow zone between the two sub-basins. Mesokurtic sediments were found in the central zone of the WSB and in front of the Due Torri Canal. Platykurtic sediments were present only in the central zone of the WSB.
- Skewness (Sk) (Figures S2d and 5d): The skewness was mostly nearly symmetrical; this occurred especially in the ESB. Sediments were strongly fine-skewed in two small-sized lenses in the WSB. Coarse-skewed sediments were observed in the centre, as well as on the western and eastern sides of the WSB. Very small-sized lenses of very coarse-skewed sediments were found on the western side of the WSB.

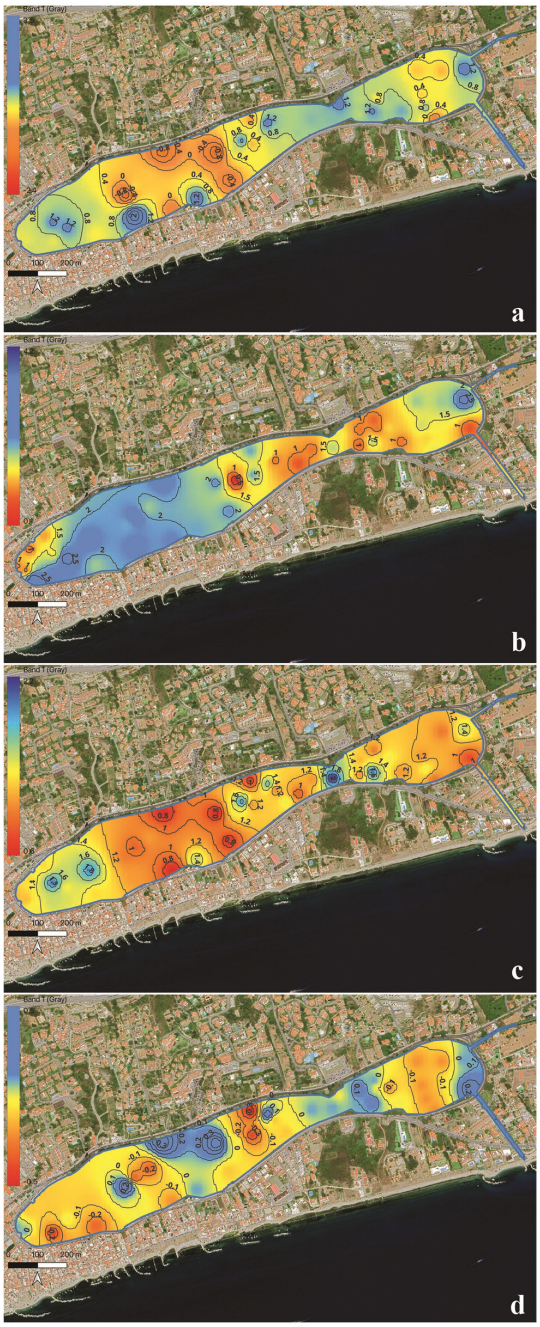


Figure 5. GIS maps of the main textural statistical data related to grain-size analyses of the coarse to fine-grained sediments. (**a**) Mean. (**b**) Sorting. (**c**) Kurtosis. (**d**) Skewness. The sign "-" corresponds to the minus sign.

The bivariate scatter plots of mean vs. skewness (Figure 6a) and mean vs. sorting (Figure 6b) indicated general overlap of the textural parameters of the LG sediments with those related to the beach sands collected along the Cape Peloro peninsula. Notwithstanding, the sorting values for most of the LG sediments were higher than those of the beach sediments.

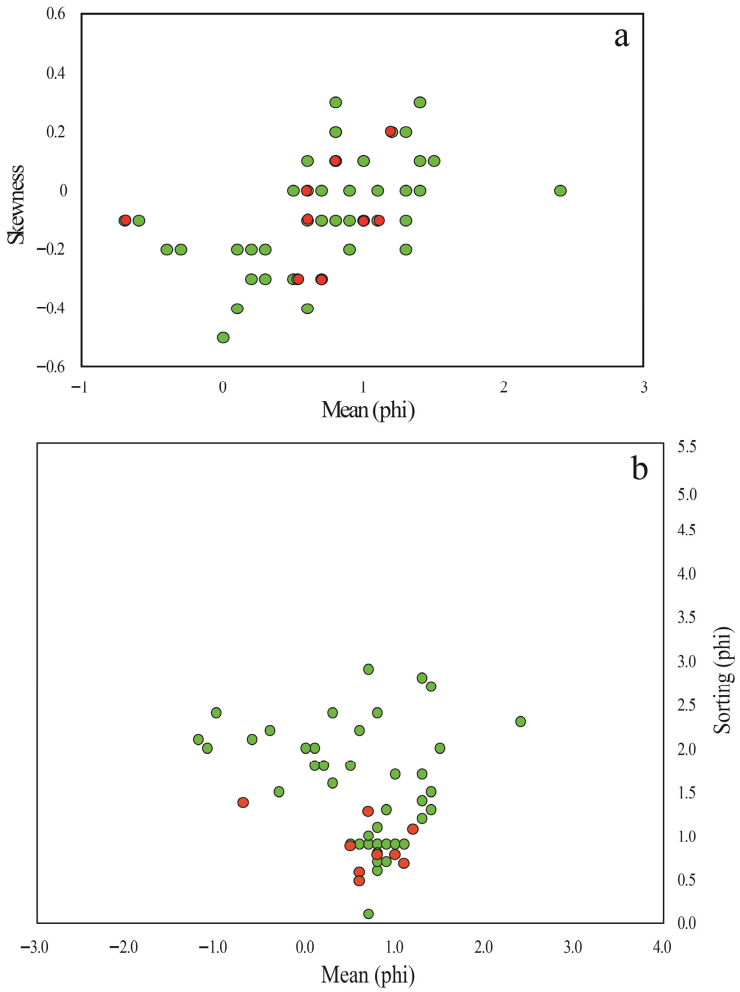


Figure 6. (**a**) Bivariate scatter plot of mean vs. skewness for the bottom sediments of LG. (**b**) Bivariate scatter plot of mean vs. sorting for the bottom sediments of LG. The Cape Peloro peninsula beach samples are also reported for comparative purposes. Symbols: LG samples, solid green circles; Cape Peloro peninsula beach samples, solid red circles.

The textural statistical parameters were further examined using a multivariate approach. The cluster analysis (Euclidean distance evaluated based on normalized values) indicated four main clusters plus a single station sliced at a 2.5 distance (Figure 7).

Several potential discriminant factors were considered (such as location, bioclast amount, farming activities, depth, etc.), whose effectiveness was verified by the one-way Anosim test. Among them, only the depth showed a moderate but statistically significant discriminating effect (Global R = 0.399; p = 0.001), allowing three main bathymetric zones to be distinguished (<2 m, 2–4 m, and >4 m depths) (Figure 7).

The first cluster included three samples collected at depths >2 m (Figure 7). Sediment grain size ranged from granules to very coarse-grained sand. The sorting was very poor. The kurtosis ranged from very platykurtic to mesokurtic. The skewness was strongly fine (Figure 7). The second cluster was formed by 17 shallow water stations at depths <2 m, plus two stations at 2–4 m and >4 m depths (Figure 7). Sediment grain size ranged from coarse- to medium-grained sand. The sorting ranged from very well to poor. The kurtosis

ranged from platykurtic to leptokurtic. Skewness ranged from coarse to nearly symmetrical (Figure 7). Although all three depth levels were represented in the third cluster, sediment features of the 12 stations (Figure 7) were almost homogeneous, ranging from coarse to very coarse-grained sand. The particle-size frequency curve indicated poorly to very poorly sorted sediments. Kg ranged from very platykurtic to mesokurtic. Moreover, sediments ranged from strongly coarse to coarse-skewed (Figure 7). Shallow water stations (<2 m depth) prevailed in the fourth cluster (9 of 13 samples), which also included one station at a 2–4 m depth and three stations at >4 m depths (Figure 7). Sediment granulometry indicated coarse to medium-grained sand. The sorting ranged from poor to very poor. The kurtosis ranged from mesokurtic to leptokurtic. The skewness ranged from coarse to strongly fine. This group probably included the most heterogeneous sediments, showing a wide range of statistical parameter values (Figure 7). Lastly, the single sample (LG06) was characterized by fine-grained sand with a very poorly sorted, platykurtic, and nearly symmetrical particle-size frequency curve (Figure 7).

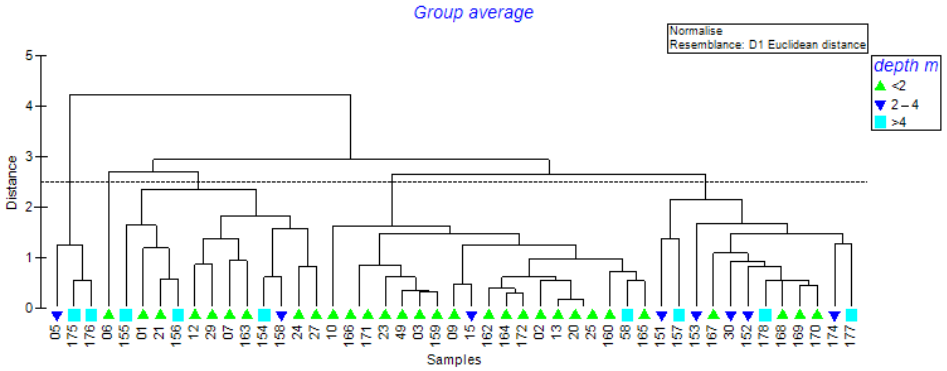


Figure 7. Cluster analysis of the bottom sediments of LG. Depth, as a discriminant factor, is evidenced (see top right). The four clusters recognized by slicing at a Euclidean distance of 2.5 are indicated.

5.2.2. Silty-to-Clayish Fractions

The silty-to-clayish fraction (~1.8%) in the total sediment samples was mainly represented by poorly sorted, medium- (~76.6%) to coarse- (~14.9%) and fine-grained (~8.5%) silts. Medium-grained silts were characterized by leptokurtic and fine-skewed distributions.

The frequency and cumulative curves (Figure S3), as well as the textural statistical parameters (Figure S4) related exclusively to the silty-to-clayish fractions of the total sediment samples, are reported in the Supplementary Materials.

The areal distributions of the textural statistical parameters (Figure 8) are described as follows.

- Mean (Mz): The fine fraction of the LG sands was mostly represented by medium-grained silts homogenously distributed in the lake. Two lenses of coarse-grained sands with minor amounts of coarse-grained silts were present on the western side of the WSB. A small lens of coarse-grained sands with minor amounts of fine-grained silts was located on the western side of the ESB. Very fine-grained silts and clays were absent in the lake sands (Figure 8a).
- Sorting (SD): The fine fraction of the LG sands was poorly sorted. A decreasing gradient sorting was observed from the ESB towards the WSB (Figure 8b).
- Kurtosis (Kg): The fine fraction of the LG sands was mostly mesokurtic and homogenously distributed. A small lens of coarse-grained sand with platykurtic silts was present in front of the Due Torri Canal. A lens of coarse-grained sands with leptokurtic silts was present on the southern side of the WSB. Values indicating strongly leptokurtic and strongly platykurtic curves were absent in the lake (Figure 8c).

- Skewness (Sk): The fine fraction of the LG sands was mostly fine-skewed and homogenously distributed. Coarse-grained sand with nearly symmetrical silts was located in the centre of the ESB and on the eastern edge of the WSB, near the narrow zone. Coarse-grained sand with strongly fine-skewed sediments mostly stayed on the southwestern side of the WSB and formed a lens on the eastern side of the WSB. Two lenses of coarse-grained sand with strongly fine-skewed silts were observed in the narrow zone and in front of the Due Torri Canal (Figure 8d).

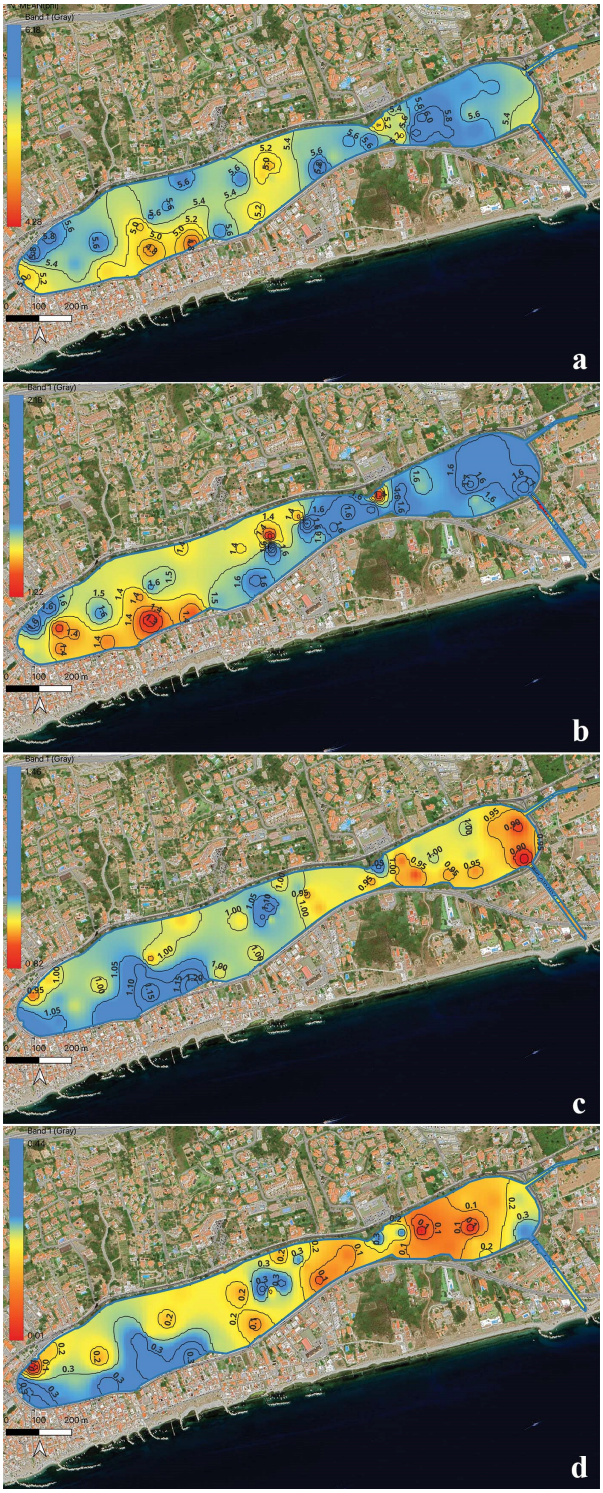


Figure 8. GIS maps of the main textural statistical data related to grain-size analyses of the fine fractions of the bottom sediments. (**a**) Mean. (**b**) Sorting. (**c**) Kurtosis. (**d**) Skewness.

5.3. Petrographic and Mineralogical Composition

Most of the analysed sediments were mainly composed of sandy grains of monomineral and polymineral assemblages. Optical observations indicated a marked prevalence of metamorphic and igneous lithoclasts (Figure 9). Metamorphic lithoclasts mainly consisted of quartz, with minor amounts of gneiss and mica schist gneiss (Figure 9). Quartz was mostly polycristalline (Figure 9a) and ranged from rounded (Figure 9a,b,h) to angular (Figure 9b–d). Angular clasts appeared very fractured (Figure 9a–f). Gneissic fragments showed typical internal schistosity and elongated shapes (Figure 9d,e,h). Igneous lithoclasts were mostly represented by well-rounded granitoids. The analysed specimens, on the basis of the quartz, feldspars, and lithics percentages, were classified as quartzo-lithic sands. No clay mineral was evidenced.

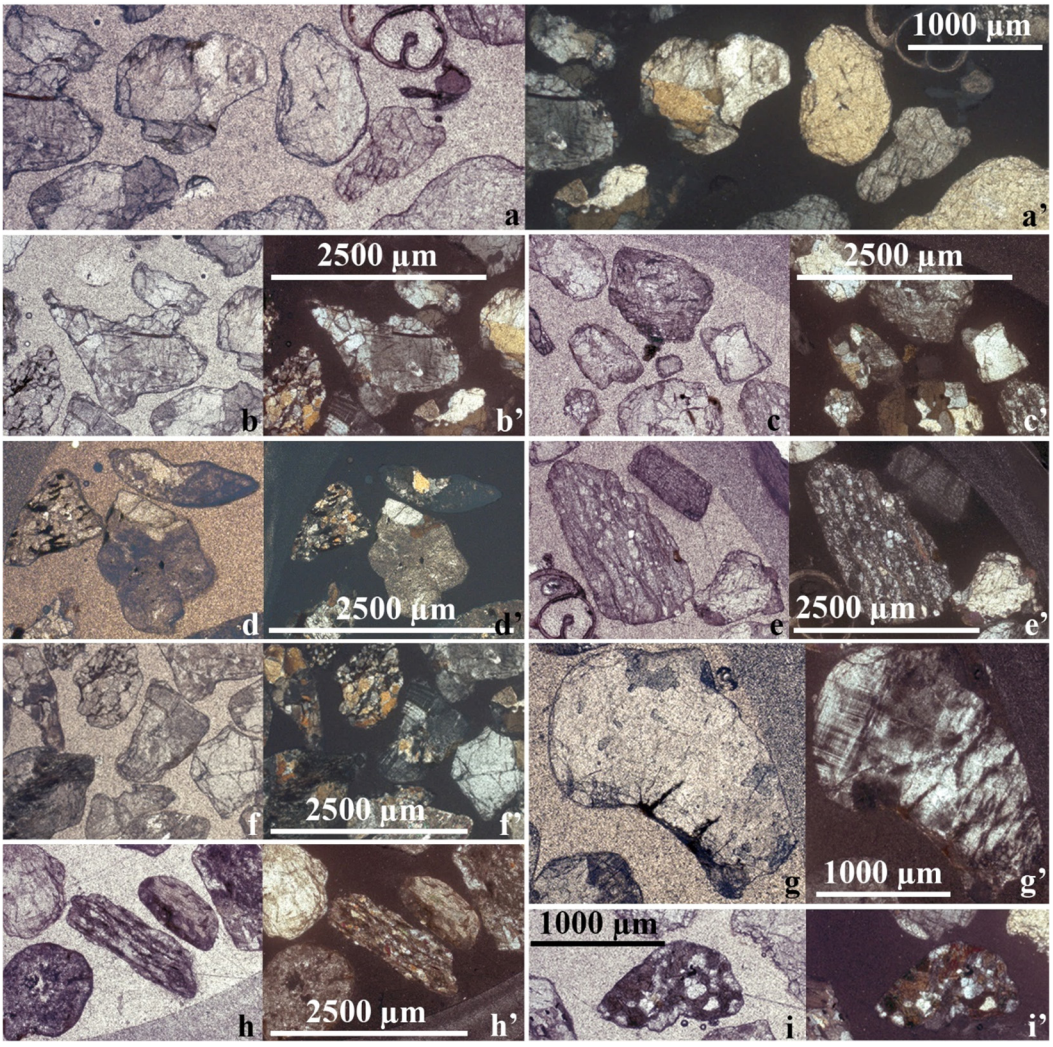


Figure 9. Thin section of bioclastic sands aggregated in epoxy resin, observed under a petrographic microscope with transmitted light (Sample LG13) ((**a**–**i**) parallel polars; (**a′**–**i′**) crossed polars). (**a**,**a′**) Subrounded and subangular grains of quartz. Skeletal remains of a spirorbid polychaete are present in the right part of the photo. (**b**,**b′**) Angular grains of quartz. A subrounded grain of gneiss is observable in the bottom left. (**c**,**c′**) Subrounded and subangular grains of quartz. A subrounded grain of gneiss is observable in the bottom right. (**d**,**d′**) Subangular grains of quartz. A subrounded grain of gneiss is observable in the middle left. (**e**,**e′**) Subrounded grain of gneiss showing schistosity. (**f**,**f′**) Subangular grains of gneiss. (**g**,**g′**) Well-rounded grain of feldspar (microcline). (**h**,**h′**) Subrounded grains of gneiss. (**i**,**i′**) Subrounded grain of gneiss.

All sediments were bioclastic, showing the occurrence of bioclasts ranging from fine-grained carbonate detritus to coarse bioclasts.

5.4. Bioclast Types

Calcareous bioclasts notably contributed to the sediment composition in almost all the examined soft sediment samples (50), especially in the coarsest fractions. The bioclast contents in the size fractions from 1 mm to over 9.5 mm ranged from <1% to 53% (mean value, 10 ± 14%). Analogous aliquots in the form of minute biogenic fragments were found in the finer granulometric fractions. The areal distribution of the bioclastic coarse fraction (Figure 10) evidenced a hotspot at high density in a well-defined area covering almost half of the WSB's eastern side. In general, the WSB's western side, the ESB, and the narrow zone between the two sub-basins showed very low contents of bioclastic coarse remains (Figure 10).

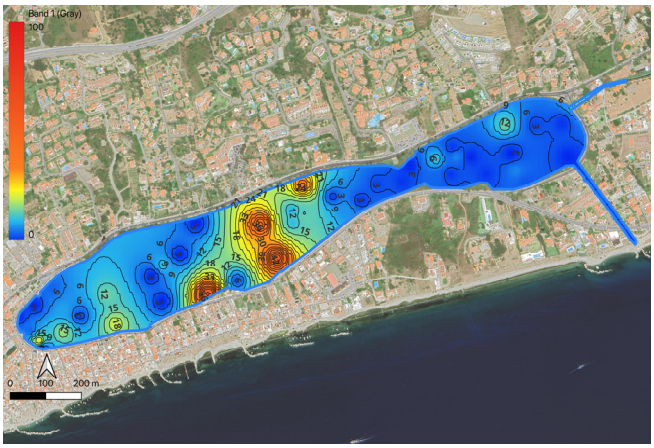


Figure 10. GIS map of the distribution related to the coarse bioclasts present in the bottom soft sediments. The concentrations are expressed as g%.

Mollusc shells—both entire and fragmented—dominated the bioclastic fraction. Sporadic remains of cirriped crustaceans and colonial serpulid polychaetes were also found.

A total of 15 mollusc taxa were recorded. All taxa were determined at the species level, except for gastropod *Haminoaea* sp. because it belongs to a genus in which a reliable determination at the species level was not possible based on the shell characteristics alone. Nine of the recorded species were gastropods, and six were bivalves. Notwithstanding, the latter, in general, were most frequently recorded. In fact, farmed clam *Polititapes aureus* occurred in 40 samples, followed by farmed cockle *Cerastoderma glaucum*, which was found in 35 samples. Among the gastropods, the most frequent one was *Steromphala adansonii*, present in 26 samples, followed by *Thericium lividulum*, found in 19 samples. Two other gastropods (*Tritia neritea* and *Tritia corniculum*) and one bivalve (*Loripes orbiculatus*) were found in 15 samples, as well as serpulid polychaetes. In decreasing order, gastropods *Hexaplex trunculus* (11 samples) and *Haminoaea* sp. (9 samples) characterized a significant number of samples, as well as the farmed clam *Ruditapes decussatus* (8 samples). Other more localized species were indicative of peculiar facies, such as bivalve *Abra segmentum*, found only in 5 samples localized in the less confined ESB, despite the fact that this species is typical of marked brackish conditions. The co-occurrence of *Gastrana fragilis* at three such stations (which indicates a lower degree of confinement) instead suggests variable energy depositional conditions. Similarly, strictly endemic gastropod *Tritia tinei* (two samples) was associated with sediments with high organic matter contents. The occurrence of congeneric species *T. reticulata* (one sample) should be considered occasional, since, to date, living specimens have exclusively been found to be associated with stocks

of clams introduced to LG for commercial purposes. Lastly, the occurrence of gastropod *Notocochlis dillwynii* (one sample) from the Due Torri Canal is in agreement with a more marked marine connotation and the dominance of intense tidal currents. The observed patch distribution of cirripeds and serpulids coincided with the occurrence of buoys and other floating objects; consequently, it did not provide significant ecological information. Unlike the latter, mollusc remains partly reflect local death assemblages; however, their composition is significantly influenced by long-standing clam farming activities, which bias species representation and abundance.

Based on the presence/absence criterion, the faunistic content was examined in terms of Bray–Curtis similarity (Figure 11). The related cluster analysis, sliced at a 40% similarity level, distinguished two main clusters of stations, plus a couple and a single station. One-way and two-way Anosim tests applied to the main potential constraints (location, bioclast amount, farming activities, and depth) indicated that only the depth had a low (Global R: 0.228) but significant discriminating effect (p: 0.1%; number of permuted statistics greater than or equal to Global R: 0), distinguishing two main bathymetric zones (<2.5 m and 2.5–4 m depths) (Figure 11).

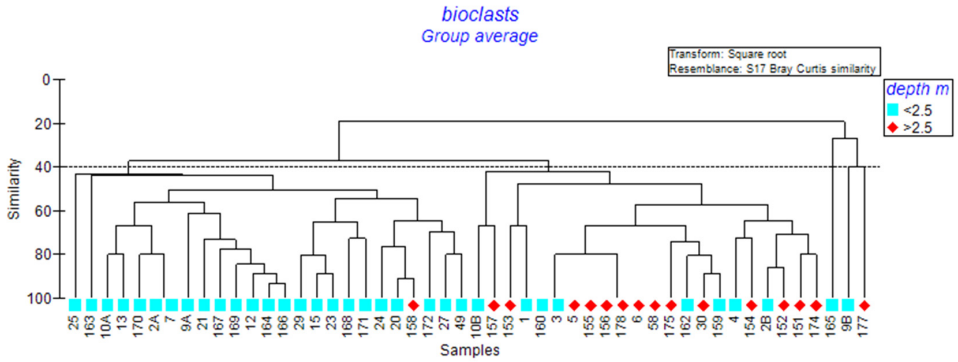


Figure 11. Bottom sediment samples clustered according to the composition of the bioclast death assemblage. Depth, as a discriminant factor, is put in evidence. The two main clusters recognized by slicing at 40% Bray–Curtis similarity are indicated.

A Simper analysis carried out on the sample groups according to depth, as a discriminant factor, indicated a similarity level of 45.40% for the group of stations at <2.5 m depths, with seven species responsible for 91% of the intra-group similarity. Among them, bivalve *Polititapes aureus* and gastropod *Steromphala adansonii* contributed 29% and 20%, respectively, together explaining almost half of the total variance. Bivalve *Cerastoderma glaucum* (15%) and gastropod *Thericium lividulum* (11%) were also relevant, followed by bivalve *Loripes orbicularis* (8%) and nassariid gastropods *Tritia corniculum* (6%) and *Tritia neritea* (4%). In contrast, the group of stations at >2.5 m depths showed a higher intra-group similarity (57%). The latter was divided into only three species, which were responsible for 91% of the intragroup similarity, half of which was due to the sole *Cerastoderma glaucum* (51%). *Polititapes aureus* contributed 35%, while no other mollusc species was significantly present. Serpulids provided a modest but significant contribution (5%). A greater number of species (11) contributed to the 61% inter-group dissimilarity, including *Ruditapes decussatus* (6%), *Hexaplex trunculus* (5%), and *Haminoaea* sp. (5%), with *S. adansonii* (13%) and *T. lividulum* (10%) being the most representative species.

Molluscs and other skeletal remains contributed to the total amount of carbonate bioclastic fractions at different degrees according to their occurrences in the examined size fractions. Accordingly, some of the five initial granulometric fractions were merged, separately considering the composition of the bioclast fractions between 1 mm and 2 mm, 4 mm and 9.5 mm, and >9.5 mm. The weight percentages of these three fractions are

shown in Figure 12. It is noted that the ratios between the different granulometric fractions were neither constant nor regular. The coarsest fraction (>9.5 mm) generally prevailed, although it was occasionally lacking. Its trend mostly agreed with that observed for the 9.5–4 mm fraction, in contrast with the 1–4 mm fraction, whose contribution was more variable. In sediments rich in bioclastic fractions, indeed, it reached high concentrations (up to 26.2% of the total samples; sample LG147), but it was also completely lacking, as in the case of sample LG175. Interestingly, each of the three fractions corresponded to a well-characterized bioclast category. Precisely, the coarsest fraction (>9.5 mm) almost entirely included shell remains of commercial *Polititapes aureus* and *Ruditapes decussatus* (Linnaeus, 1758) clams. Large gastropod *Hexaplex trunculus*, a carnivore preying on bivalve molluscs, was only occasionally recorded. Instead, the 9.5–4 mm bioclastic fraction was dominated by the commercial cockle (*Cerastoderma glaucum*). However, low concentrations of other non-commercial species, such as *Loripes orbiculatus*, *Gastrana fragilis*, and *Abra segmentum*, can be found, as well as sporadic cirripeds. Lastly, the 4–1 mm fraction showed almost exclusively gastropod remains, primarily due to small-sized species or, less frequently, juveniles. In general, each gastropod species was represented by a few specimens, except for *Steromphala adansonii*, whose high numbers in scattered stations agreed with the local abundance of both benthic and floating macrophytes. Relatively abundant minute fragments of serpulid were also found.

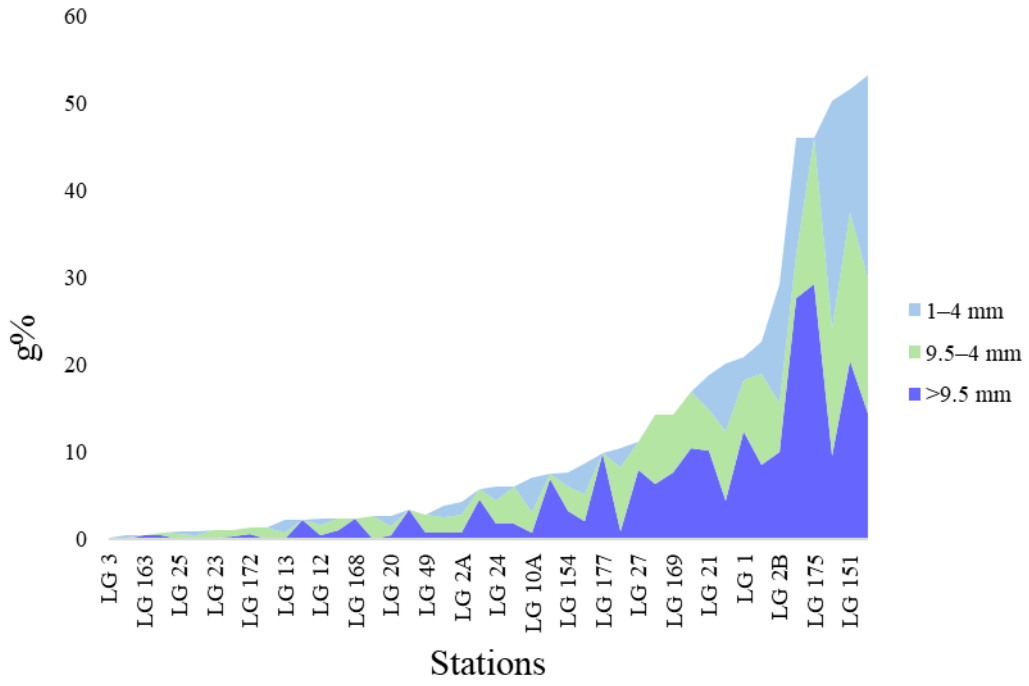


Figure 12. The bioclastic content (g%) of each sediment sample, reported separately for the three considered size classes.

5.5. Geological Map

A geological map of LG's bottom bed is shown in Figure 13. The bed of the lake bottom was mainly composed of bioclastic coarse-grained sand. Small lenses of bioclastic medium and very coarse-grained sand also appeared to be randomly distributed among the coarse-grained sand. A more consistent lens of bioclastic very coarse-grained sand with bioclastic gravel appeared to be arranged along a NW–SE trend in the deep sector of the WSB's central area.

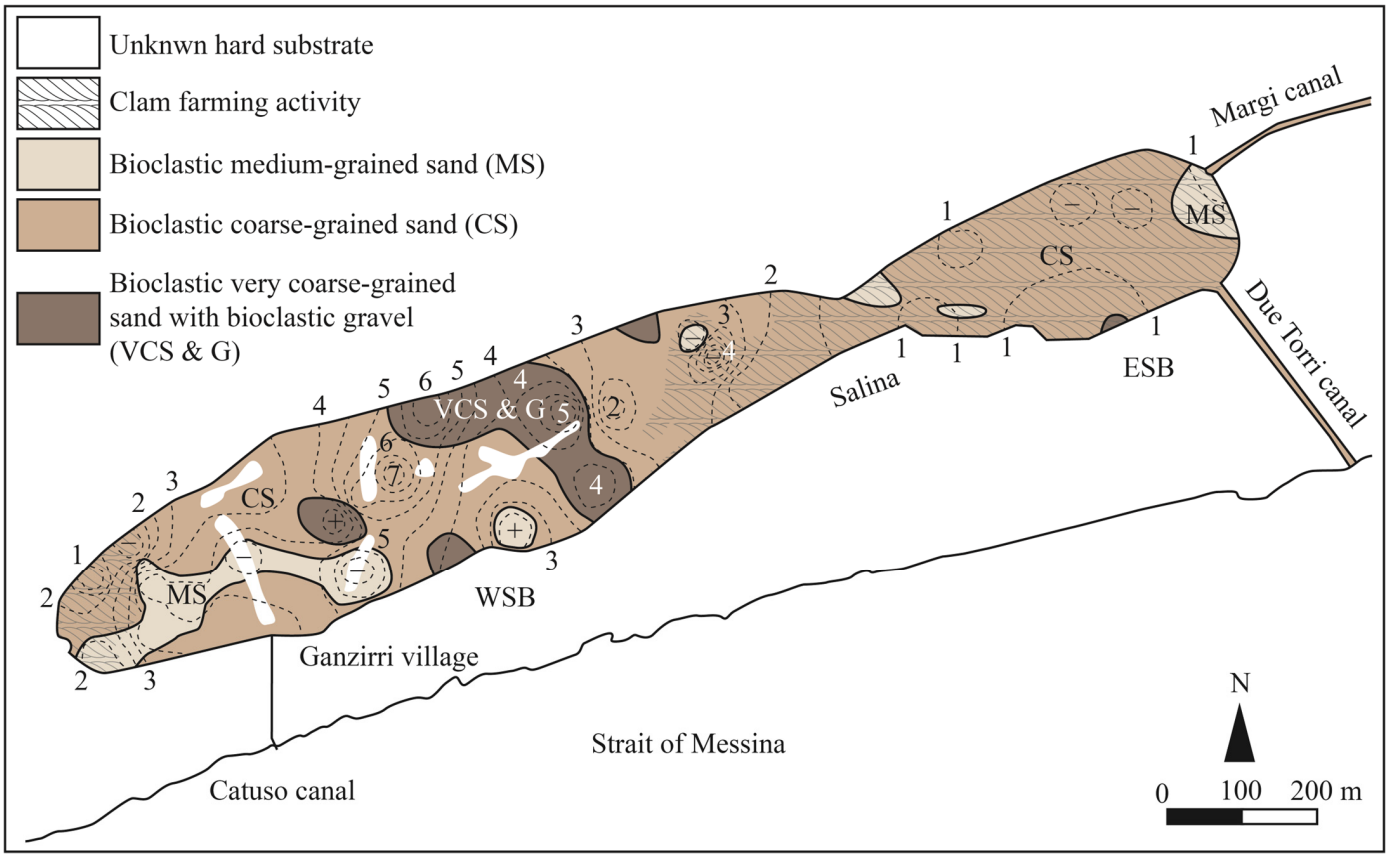


Figure 13. Geological map of the bottom bed of Lake Ganzirri based on QGIS elaborations. The bathymetric contour lines (black dotted line) are in meters (spacing: 0.5 m). The area affected by clam farming activity is at shallow depths and localized mostly between the ESB and the WSB's eastern side.

6. Discussion

6.1. Morpho-Bathymetry and Structural Geology

An updated morpho-bathymetric map of LG was provided in the present paper after 70 years [34]. The previous map was very simplified, showing homogenous decreasing depths with concentric contour-line patterns. The elevated number of measurement stations allowed for the identification of some cliffs on the bottom of the WSB, which could be interpreted as evidence of a small-sized NNE–SSW-trending graben (within the main ENE–WSW-trending Ganzirri graben) that had not been detected until now. Notwithstanding, this hypothesis should be validated by further geophysical surveys and core drilling because other competing hypotheses, such as erosional lines or anthropogenic transformation, cannot be excluded.

6.2. Geology, Sedimentology, and Mineralogy

The geological map of the lake-bottom sediments (Figure 13) provided a clear and effective synthesis of bathymetry and sediment distribution, which could significantly enhance the interpretation of depositional patterns.

Most of the bottom bed was found to be composed of sub-mature sediments, being made up of poorly sorted coarse-grained sand with very low contents in the finest fractions (prevailing medium-grained silts). The clastic fraction showed a quartzo-lithic composition with a constant presence of biogenic carbonates (bioclast fragments and entire shells) in all grain-size fractions. Minor lenses of very coarse-grained sand (very rich in bioclasts) with gravel and medium-grained sand were also detected. Sediments were mostly characterized by leptokurtic and nearly symmetrical distributions. A general heterogeneity in the textural

statistical parameters was ascertained. The sediments of the bottom bed were attributed to the most recent facies association (FA3) [34], whose base was inferred to the end of the 18th century, i.e., when the lagoon's isolation was interrupted by the digging of artificial canals connecting the lakes to the sea [34]. It is hypothesized in the present research that the clastic input to LG could be derived from the main connection with the Ionian Sea (Due Torri Canal) during this phase. Alternatively, tidal currents, whose energy abruptly drops into the lake, may have been responsible for introducing sandy sediments and removing resuspended silts to and from the lake, respectively. Although stream flows are not actually present, periodic floodings due to heavy rainfall could have occasionally transported moderate amounts of sediments into the lake. Notwithstanding the fact that the lake is surrounded by a ring road on a highly urbanized territory (which significantly limits clastic contributions), such inputs could have reached the lake margins because of under-dimensioned white-water sewers. As concerns the longshore and offshore redistribution of clastic sediments by waves, the limited extent of LG presumably could prevent the formation of significant wave motions. In contrast, the action of the winds, which may be very strong in the Strait of Messina, could have interfered with the shallow water bottom, stirring up sediments, especially in the shallowest zones of the WSB, where the bottom is free from aquatic vegetation. The deeper zone of the WSB, despite being a natural site of organic matter decanting, did not appear to be affected by downslope transport of finer sediments or turbiditic flows. The in situ production of deposits rich in biogenic carbonate fractions is in accordance with the local high biological productivity evidenced in LG [37]. Lastly, water stagnation, hyper-evaporation, and supersaturation conditions, which can indicate salt precipitation, were not evidenced in LG, although a site denoted as "Salina", surrounding the southern side of the ESB (Figure 13), could testify to an ancient hyper-saline.

The texture identified by Palli et al. [34] in the bottom bed is in partially agreement with the results of our study, being simply ascribed to medium-grained sands. However, there is agreement in the data concerning the degree of confinement. As a matter of fact, the studied sediments formed under high-energy conditions in an open-lagoon environment.

No evident relationships between the grain-size distributions and depths were detected, except for a hectometre-long lens of medium-grained sand stretched along a small valley present on the westernmost side of the WSB. Indeed, a decreasing grain-size gradient from coarse- to medium-grained sand, associated with a decreasing depth gradient, was evidenced. It may be hypothesized that wind-induced higher water-flow energy conditions could have conditioned the NW–SE-trending main lens of very coarse-grained sand with gravel (Figure 13).

According to the multivariate statistical analyses, the main potential constraints, such as depth, location, exposure, farming activities, bioclast concentration, and different species composition of the bioclastic >2 mm fraction, did not evidence recognizable effects. The observed heterogeneity in textural and bioclastic distributions likely reflects the combined effects of ongoing anthropogenic disturbance (e.g., clam farming) and natural hydrodynamic processes operating at short temporal scales. Some natural effects, such as those tied to the lake–sea connection, were recognized, but the most severe causes of alteration could be found in the secular anthropogenic pressures. In fact, a deep modification of LG's original depositional system could be seen in the ancient custom of creating sandy mounds in the lake's shallow areas by transferring beach sediments into the lake for clam farming purposes. Tied to this traditional activity, continuous reworking of the shallow bottom beds may have also occurred. Similarly, clam farming activities could be responsible for altered bioclastic deposition, resulting from the harvesting of living molluscs and clearing away of empty shells. However, the strong affinities of the grain-size cumulative curves (Figure S1a)

and the bivariate scatter plots (Figure 6) related to the lake sediments and beach deposits of the surrounding coasts cannot be explained only in terms of anthropogenic disturbance.

On a secular-to-millennial temporal scale, another factor that could have played an important role in determining the observed spatial heterogeneity in sand grain sizes and textures could be found in natural exceptional events, such as extreme sea storms or tsunamis. As reported by historical sources, in fact, the tsunami associated with the disastrous seismic event of 5 February 1783 [51–53] (Figure 2) affected the Cape Peloro lagoon, over-running both LG and Lake Faro with nearby sea waters and sediments. Exceptional high-energy events, such as historical tsunamis documented for the area, could have contributed locally to sediment reworking; however, diagnostic sedimentological criteria for tsunamiites were not searched for at this stage of research, and this interpretation remains speculative.

6.3. Faunistic Content

The rich malacofauna found in the examined sediments was descriptive of the current ecological asset. The detected species were all characteristic of brackish environments, including exclusively endemic *Tritia tinei*. Due to their high eury-valence, they were widely diffused in the lake bottom. Some evidence of diversification was also recognized, especially in the case of less common species, owing to their ties to different confinement grades of the environment (sensu Guelorget and Perthuisot [54]). According to bathymetry, the low species diversity and the scarce bioclastic fraction indicate poor biotic conditions in the zone at >2 m depths with respect to the high productivity of the lake bottom at depths < 2 m. Moreover, the high amounts of edible mollusc shells, in general, were a clear consequence of the diffuse clam farming activities that occurred over the centuries in the lagoon. The differentiated distribution of species among the examined grain-size fractions suggests a differentiated contribution of human activities related to clam farming. The highest concentrations of commercial clam remains were mostly found close to the farmed parcels (mostly concentrated in the ESB and the WSB's eastern side; Figure 13), enriching the modern soft sediments with coarse-grained bioclast "waste" (Figure 10). Elsewhere, the bioclastic fraction was poor but well characterized and coherent with a natural brackish environment and weakly reworked bottom sediments.

6.4. Comparative Analyses Between the Sediment Features and the Available Chemical Data

Different grades and typologies of human impact may be expected in LG. Accordingly, the contextual investigation of chemical elements [15] provided useful basic information. A synthetic map elaborated from this data (Figure 14) showed the areal distribution of five main geochemical hotspots related, in the complex, to Zn, Pb, Tl, Ni, Cu, Cr, and Cd heavy metals. The easternmost hotspot (H1 in Figure 14), including the areas of the Margi Canal and Due Torri Canal, was located on the eastern edge of the ESB; this hotspot was the most consistent, including the presence of Zn (in front of Margi Canal), Pb (in front of both Margi Canal and Due Torri Canal; maximum value: LG21), Tl (in front of Margi Canal), and Cd (in front of Due Torri Canal; maximum value: LG13). Two minor hotspots (H2 and H3 in Figure 14) were evidenced in the narrow zone between the sub-basins; H2 and H3 showed the occurrence of all the studied heavy metals, with the presence of Zn, Pb, Cu (maximum value: LG25), Cr, and Cd. The H4 western hotspot, located in the centre of the WSB, was the most extensive and related to Zn (maximum value: LG07), Tl, and Cr (maximum value: LG07). The westernmost hotspot (H5 in Figure 14) was on the edge of the WSB; this hotspot was related to Pb, Tl (maximum value: LG02), and Cr.

No clear spatial correspondence was observed between the distributions of sedimentological and ecological features (Figures 3b, 5 and 8), and the mapped heavy metal hotspots

(H1–5 in Figure 14). In contrast, a significant match between the main heavy metal hotspots (Figure 14) and the hotspots of a few metals (Al, Fe, and Mg) [15] was evidenced.

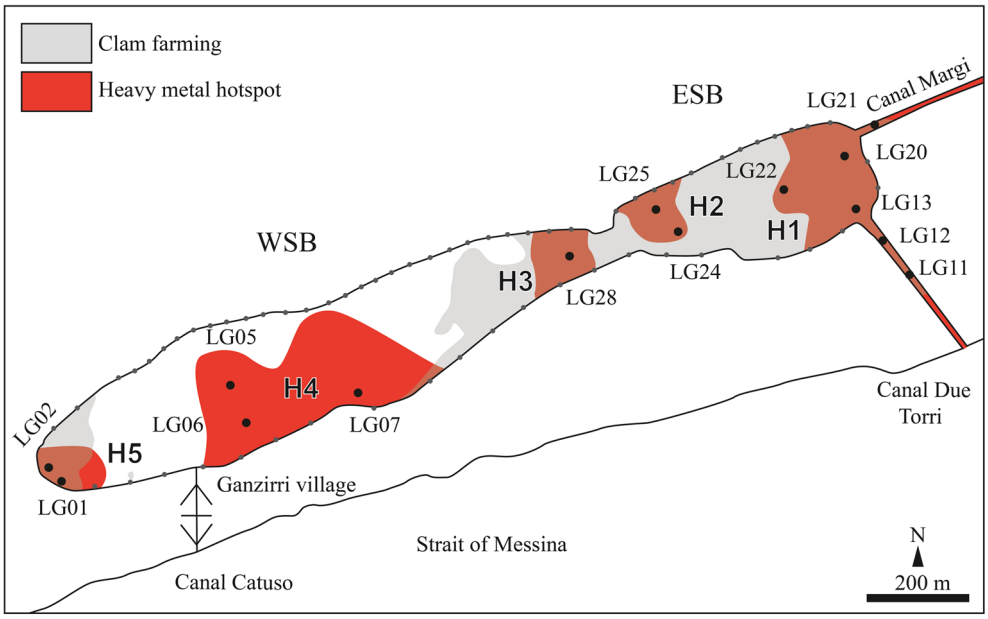


Figure 14. Synthetic map reconstructing the main heavy metal hotspots (H1–5) in the bottom soft sediments of Lake Ganzirri and canals (modified after [15]). The samples (LG, solid black circle) showing the most elevated concentrations are also reported. The discharge pipes of the surface waters are reported along the lake's shoreline (solid grey circles).

For a full discussion of these data and the correlation statistics, the authors refer to the research of Cigala et al. [15].

It must be underlined that the metal concentration ranges [15] were all compatible with pre-industrial background values. Moreover, the concentrations normalized to geogenic metals, being very low, suggest a prevalent natural origin for the heavy metals. Indeed, their presence in the bioavailable fraction of the sediments should be geogenic and due to the release of metals from the source rocks. Chemical–physical weathering due to rainwater infiltrating into the bedrock (actual alluvial deposits, middle Pleistocene sediments, and high-grade metamorphic rocks—Aspromonte Unit; Figure 1) and outcropping in the upstream surrounding areas could be responsible for delivering metals that could be transferred into the sediments of the lake-bottom bed. Low concentrations of heavy metals in LG waters found in the past [43] would better agree with a mostly natural origin of these metals. Very low concentrations of metals recently found in edible filtering feeder clams of LG [14] further support this hypothesis.

The absence of high values of the heavy metal concentrations in the bioavailable fraction of the sediments, as well as the lack of an evident connection with the sedimentology factors, could be explained by the high mobility and low retaining capacities of the heavy metals in the sediment's coarse- to very coarse-grained textures, devoid of clayish fractions. Indeed, heavy metal accumulation in sediments mainly depends on the surface-area availability of particles. Fine-grained sediments are typically characterized by higher specific surface areas and greater proportions of clay minerals, organic matter, or Fe–Mn oxides, enhancing the adsorption and retention capacity of metals [55].

Coarse- to very coarse-grained sand dominated by quartzo-lithic grains with low surface area and limited reactive sites, as the study sediments, may result in a reduced capacity for metal sorption. Additionally, the prevalence of poorly sorted sediments promotes higher permeability and pore–water exchanges, increasing the potential for metal

remobilization rather than long-term retention. Finally, a further factor to consider is that the study sediments, being associated with a high-energy depositional environment, such as that of shallow open lagoons, may experience frequent resuspensions and sediment reworkings, inhibiting the accumulation of heavy metals.

7. Conclusions

A first detailed geological map of the lake's actual bottom bed, an updated morpho-bathymetric map, and a topographic cross-section of the lake bottom, together with the first detailed maps of the main sedimentological statistical parameters (mean, sorting, kurtosis, and skewness) of the bottom bed, provided a solid background to better understand the geological, sedimentological, and ecological processes affecting LG and the current coastal lake systems. The mixed composition of the bottom clastic sediments due to quartzo-lithic sands and consistent amounts of calcareous bioclasts (mainly connected with clam farming) was also evidenced for the first time in the studied sediments. The heterogeneous textures of the bottom-bed sediments were indicative of an open-lagoon environment dominated by high-energy conditions. The latter, established after the re-connection of the lagoon waters with the sea in the 18th century, were analogous to those characterising the lagoon during the early Bronze Age. Lastly, considering the absence of evident spatial correlations between the areal distribution of the textural parameters and the known heavy metal hotspots, as well as the correlation between the same heavy metal hotspots and some metals (Al, Fe, and Mg), a geogenic origin for the heavy metals may be presumed. Consequently, significant anthropogenic contamination can be excluded.

Based on the above, the present research proposed a multi-disciplinary approach based on the comparison of spatial maps and bivariate and multivariate statistical data that could provide a useful tool for assessing the natural or anthropogenic source of contaminants in sediments of vulnerable coastal lake systems, allowing for a better evaluation of ecological risk. In conclusion, the integration of sedimentological data, ecological indicators, and spatial analyses presented here may provide a significant contribution to the understanding of modern coastal lagoon systems and support improved insights into the evolution and management of transitional environments.

Supplementary Materials: The following supporting information can be downloaded at: https://www.mdpi.com/article/10.3390/quat9010009/s1, Table S1. Main textural feature (SD: sorting, kurtosis, skewness, and mean) of the total sediments of Lake Ganzirri. Figure S1. Sediments of Lake Ganzirri. (a) Cumulative retained oversize curves related to the grain-size distribution of the total sediment samples (solid black lines). The granulometric zone of the Lake Ganzirri deposits is outlined with the light-blue dotted line (data related to the neighbouring beaches are reported with the red dotted line). (b) Ternary diagram (gravel, sand, and mud) showing the composition of the total sediment samples. Figure S2. Main textural statistical data of the total sediment samples: (a) mean; (b) sorting; (c) kurtosis; (d) skewness. Dataset based on 46 samples. Figure S3. (a) Frequency and (b) cumulative curves related to the silty-to-clayish fraction of the total sediment samples collected on the LG bottom. The graphs were obtained using the workstation associated with the Mastersizer laser diffractometer. Figure S4. Main statistical data of the silty-to-clayish fraction of the total bottom sediments: (a) mean; (b) kurtosis; (c) skewness. Dataset based on 46 samples. The frequency % of each category for all considered parameters is represented.

Author Contributions: Conceptualization, R.S. and S.G.; methodology, R.S. and S.G.; software, M.G.Y., M.A., R.K.M. and S.Z.; validation, R.S. and S.G.; formal analysis, R.S., M.G.Y., A.C.M., R.K.M. and S.G.; investigation, R.S., M.G.Y., A.C.M. and R.K.M.; data curation, M.G.Y., M.A. and R.K.M.; writing—original draft preparation; R.S. and S.G.; writing—review and editing, R.S. and S.G.; visualization, R.S., M.G.Y., A.C.M., M.A., R.K.M., S.Z. and S.G.; supervision, R.S. and S.G. All authors have read and agreed to the published version of the manuscript.

Funding: This work was supported by PO FEAMP (Fondo Europeo per gli Affari Marittimi e la Pesca) 2014/2020 measure 2.5.1.

Data Availability Statement: The original contributions presented in this study are included in the article/Supplementary Material. Further inquiries can be directed to the corresponding author.

Acknowledgments: The authors wish to give special acknowledgement to Maria Letizia Molino (Oriented Reserve of Cape Peloro, Metropolitan City of Messina) for permissions and logistical support, and to Salvatore Ruello (Società cooperativa Lago Grande di Ganzirri) for assistance during field activities. The reviewers are sincerely acknowledged for their insightful comments and very constructive suggestions, which substantially improved this paper. The authors are also grateful to the Academic Editor and the Assistant Editor.

Conflicts of Interest: The authors declare no conflicts of interest.

Abbreviations

The following abbreviations are used in this manuscript:

LG	Lake Ganzirri
LF	Lake Faro
ESB	Eastern sub-basin
WSB	Western sub-basin

References

1. Maccarrone, V.; Scandura, P.; La Rosa, S.D. The Integrated Coastal Zone Management in the Anthropocene. In *Coastal Sustainability Insights from Southeast Asia and Beyond*; Maccarrone, V., Fadzil Akhir, M., Eds.; Springer Nature: Cham, Switzerland, 2024; Volume 39, pp. 1–20. [CrossRef]
2. Young, A.F. Coastal megacities, environmental hazards and global environmental change. In *Megacities and the Coast: Risk, Resilience and Transformation*; Pelling, M., Blackburn, S., Eds.; Earthscan from Routledge: London, UK, 2014; Volume 3, pp. 70–99. [CrossRef]
3. Dias, G.M.; Edwards, G.C. Differentiating natural and anthropogenic sources of metals to the environment. *Hum. Ecol. Risk Assess.* **2003**, *9*, 699–721. [CrossRef]
4. Masindi, V.; Mkhonza, P.; Tekere, M. Sources of heavy metals pollution. In *Remediation of Heavy Metals*; Springer Nature: Cham, Switzerland, 2021; pp. 419–454. [CrossRef]
5. Kostka, A.; Leśniak, A. Natural and anthropogenic origin of metals in lacustrine sediments; assessment and consequences—A case study of Wigry lake (Poland). *Minerals* **2021**, *11*, 158. [CrossRef]
6. Umgiesser, G.; Ferrarin, C.; Cucco, A.; De Pascalis, F.; Bellafiore, D.; Ghezzo, M.; Bajo, M. Comparative hydrodynamics of 10 Mediterranean lagoons by means of numerical modeling. *J. Geophys. Res. Oceans* **2014**, *119*, 2212–2226. [CrossRef]
7. Gooch, G.D. *Coastal Lagoons in Europe: Integrated Water Resource Strategies*; Lillebø, A.I., Stalnacke, P., Gooch, G.D., Eds.; IWA Publishing: London, UK, 2015; pp. 1–256.
8. Longhitano, S.G.; Della Luna, R.; Milone, A.L.; Cilumbriello, A.; Caffau, M.; Spilotro, G. The 20,000-years-long sedimentary record of the Lesina coastal system (southern Italy): From alluvial, to tidal, to wave process regime change. *Holocene* **2016**, *26*, 678–698. [CrossRef]
9. Morales-Marin, L.A.; Carr, M.; Sadeghian, A.; Lindenschmidt, K.E. Climate change effects on the thermal stratification of Lake Diefenbaker, a large multi-purpose reservoir. *Can. Water Resour. J.* **2021**, *46*, 1–16. [CrossRef]
10. Regione Siciliana. Riserva Naturale Laguna di Capo Peloro. Available online: https://orbs.regione.sicilia.it/aree-protette/riserve-naturali-siciliane/164-riserva-naturale-orientata-laguna-capo-peloro.html (accessed on 2 July 2025).
11. Somma, R.; Spoto, S.E.; Giacobbe, S. Geological and structural framework, inventory, and quantitative assessment of geodiversity: The case study of the lake Faro and lake Ganzirri global geosites (Italy). *Geosciences* **2024**, *14*, 236. [CrossRef]
12. Somma, R.; Giuffrè, E.; Amonullozoda, S.; Spoto, S.E.; Giacobbe, A.; Giacobbe, S. Geological and Ecological Insights on the Lake Faro Global Geosite Within the Messina Strait Framework (Italy). *Geosciences* **2024**, *14*, 319. [CrossRef]
13. Di Bella, G.; Litrenta, F.; Potortì, A.G.; Giacobbe, S.; Nava, V.; Puntorieri, D.; Lo Turco, V. Plasticizers and Bisphenols in Sicilian Lagoon Bivalves, Water, and Sediments: Environmental Risk in Areas with Different Anthropogenic Pressure. *Environments* **2025**, *12*, 305. [CrossRef]
14. Giacobbe, S.; Nava, V.; Sgrò, B.; Scarpa, F.; Sanna, D.; Casu, M.; Di Bella, G. Mineral content in clam species from Sicily and Sardinia: A geographical, temporal and species-specific statistical comparison. *Chemosphere* **2025**, *377*, 144328. [CrossRef]

15. Cigala, R.M.; Crea, F.; Somma, R.; De Stefano, C.; Ghanadzadeh Yazdi, M.; Giacobbe, S. Determination of potential contaminants in sediments from Lake Ganzirri brackish pond (Capo Peloro lagoon, Italy) by different instrumental techniques. *J. Environ. Chem. Eng.* 2026; *submitted*.
16. Miall, A.D. (Ed.) *Principles of Sedimentary Basin Analysis*, 3rd ed.; Springer: Berlin/Heidelberg, Germany, 2000; pp. 1–616. [CrossRef]
17. Nichols, G. *Sedimentology and Stratigraphy*, 2nd ed.; Wiley-Blackwell, John Wiley & Sons: Hoboken, NJ, USA, 2009; pp. 1–432.
18. Reading, H.G. *Sedimentary Environments: Processes, Facies and Stratigraphy*; Reading, H.G., Ed.; John Wiley & Sons: Hoboken, NJ, USA, 2009; pp. 1–688.
19. Allen, J.R. *Principles of Physical Sedimentology*; Allen, J.R., Ed.; Springer Science & Business Media, Blackburn Press: Caldwell, NJ, USA, 2012; pp. 1–272.
20. Boggs, S. *Principles of Sedimentology and Stratigraphy*, 5th ed.; Boggs, S., Ed.; Pearson Education Limited: Harlow, Essex, UK, 2014; pp. 1–676.
21. Donato, S.V.; Reinhardt, E.G.; Boyce, J.I.; Pilarczyk, J.E.; Jupp, B.P. Particle-size distribution of inferred tsunami deposits in Sur Lagoon, Sultanate of Oman. *Mar. Geol.* **2009**, *257*, 54–64. [CrossRef]
22. Bonardi, G.; Giunta, G.; Liguori, V.; Perrone, V.; Russo, M.; Zuppetta, A. Schema geologico dei Monti Peloritani. *Boll. Soc. Geol. Ital.* **1976**, *95*, 49–74.
23. Cirrincione, R.; Fazio, E.; Fiannacca, P.; Ortolano, G.; Pezzino, A.; Punturo, R. The Calabria-Peloritani Orogen, a composite terrane in Central Mediterranean; Its overall architecture and geodynamic significance for a pre-Alpine scenario around the Tethyan basin. *Period. Mineral.* **2015**, *84*, 701–749. [CrossRef]
24. Catalano, S.; Cirrincione, R.; Mazzoleni, P.; Pavano, F.; Pezzino, A.; Romagnoli, G.; Tortorici, G. The effects of a Meso-Alpine collision event on the tectono-metamorphic evolution of the Peloritani mountain belt (eastern Sicily, southern Italy). *Geol. Mag.* **2018**, *155*, 422–437. [CrossRef]
25. Somma, R. The Inventory and Quantitative Assessment of Geodiversity as Strategic Tools for Promoting Sustainable Geoconservation and Geo-Education in the Peloritani Mountains (Italy). *Educ. Sci.* **2022**, *12*, 580. [CrossRef]
26. Lentini, F.; Catalano, S.; Carbone, S. *Note Illustrative della Carta Geologica della Provincia di Messina Scala 1: 50.000*; S.EL.CA.: Firenze, Italy, 2000; pp. 1–70.
27. Segre, A.G.; Bagnala, R.; Sylos Labini, S. Holocene evolution of the Pelorus headland, Sicily. *Quat. Nova* **2004**, *8*, 69–78.
28. Perri, F.; Dominici, R.; Le Pera, E.; Chiocci, F.L.; Martorelli, E. Holocene sediments of the Messina Strait (southern Italy): Relationships between source area and depositional basin. *Mar. Pet. Geol.* **2016**, *77*, 553–566. [CrossRef]
29. Somma, R. Petrographic and Textural Characterization of Beach Sands Contaminated by Asbestos Cement Materials (Cape Peloro, Messina, Italy): Hazardous Human-Environmental Relationships. *Geosciences* **2024**, *14*, 167. [CrossRef]
30. Bottari, A.; Bottari, C.; Carveni, P.; Giacobbe, S.; Spanò, N. Genesis and geomorphologic and ecological evolution of the Ganzirri salt marsh (Messina, Italy). *Quat. Int.* **2005**, *140–141*, 150–158. [CrossRef]
31. Guarnieri, P.; Pirrotta, C. The response of drainage basins to the late Quaternary tectonics in the Sicilian side of the Messina Strait (NE Sicily). *Geomorphology* **2008**, *95*, 260–273. [CrossRef]
32. Doglioni, C.; Ligi, M.; Scrocca, D.; Bigi, S.; Bortoluzzi, G.; Carminati, E.; Cuffaro, M.; D'Oriano, F.; Forleo, V.; Muccini, F. The tectonic puzzle of the Messina area (southern Italy): Insights from new seismic reflection data. *Sci. Rep.* **2012**, *2*, 970. [CrossRef]
33. Bottari, C.; Carveni, P. Archaeological and historiographical implications of recent uplift of the Peloro Peninsula, NE Sicily. *Quat. Res.* **2009**, *72*, 38–46. [CrossRef]
34. Palli, J.; Monaco, L.; Bini, M.; Cosma, E.; Giaccio, B.; Izdebski, A.; Masi, A.; Mensing, S.; Piovesan, G.; Rossi, V.; et al. The recent evolution of the salt marsh 'Pantano Grande' (NE Sicily, Italy): Interplay between natural and human activity over the last 3700 years. *J. Quat. Sci.* **2024**, *39*, 327–339. [CrossRef]
35. Palli, J.; Fiolna, S.; Bini, M.; Cappella, F.; Izdebski, A.; Masi, A.; Zanchetta, G. The human-driven ecological success of olive trees over the last 3700 years in the Central Mediterranean. *Quat. Sci. Rev.* **2025**, *356*, 109313. [CrossRef]
36. Manganaro, A.; Pulicanò, A.; Sanfilippo, G.M. Temporal evolution of the area of Capo Peloro (Sicily, Italy) from pristine site into urbanized area. *Transit. Waters Bull.* **2011**, *5*, 23–31. [CrossRef]
37. Leonardi, M.; Azzaro, F.; Azzaro, M.; Caruso, G.; Mancuso, M.; Monticelli, L.S.; Zaccone, R. A multidisciplinary study of the Cape Peloro brackish area (Messina, Italy): Characterisation of trophic conditions, microbial abundances and activities. *Mar. Ecol.* **2009**, *30*, 33–42. [CrossRef]
38. Caruso, G.; Leonardi, M.; Monticelli, L.S.; Decembrini, F.; Azzaro, F.; Crisafi, E.; Vizzini, S. Assessment of the ecological status of transitional waters in Sicily (Italy): First characterisation and classification according to a multiparametric approach. *Mar. Pollut. Bull.* **2010**, *60*, 1682–1690. [CrossRef] [PubMed]
39. Sanfilippo, M.; Albano, M.; Manganaro, A.; Capillo, G.; Spanò, N.; Savoca, S. Spatiotemporal organic carbon distribution in the Capo Peloro Lagoon (Sicily, Italy) in relation to environmentally sustainable approaches. *Water* **2022**, *14*, 108. [CrossRef]

40. Ferrarin, C.; Bergamasco, A.; Umgiesser, G.; Cucco, A. Hydrodynamics and spatial zonation of the Capo Peloro coastal system (Sicily) through 3-D numerical modeling. *J. Mar. Syst.* **2013**, *117–118*, 96–107. [CrossRef]
41. Gianguzza, A.; Mannino, M.R.; Olivo, A.; Orecchio, S. Occurrence and concentration of PAHS in clams and sediments of the marine coastal lagoon of Ganzirri (Italy). Extraction, GC-MS analysis, distribution and sources. *Fresenius Environ. Bull.* **2006**, *15*, 1026–1033.
42. Caristi, C.; Cimino, G.; Ziino, M. Inquinamento da metalli pesanti—Nota VI Indagine sul grado di contaminazione delle acque e dei sedimenti dei laghi di Faro e di Ganzirri (Messina). *Atti Soc. Pelorit. Sci. Fis. Mat. Nat.* **1980**, *26*, 203–214.
43. Lo Coco, F.; Lanuzza, F.; Adami, G.; Cappellano, G.; Cozzi, F.; Mondello, F. La qualità delle acque dei laghi di Faro e di Ganzirri (Messina) adibiti a miticoltura. Dosaggio di metalli pesanti. In Proceedings of the la Qualità dei Prodotti per la Competitività delle Imprese e la Tutela dei Consumatori, XXII Congresso Nazionale di Merceologia, Università Roma Tre, Roma, Italy, 2–4 March 2006.
44. Abbruzzese, D.; Genovese, S. Osservazioni geomorfologiche e fisico-chimiche sui laghi di Ganzirri e di Faro. *Boll. Pesca Piscic. Idrobiol.* **1952**, *7*, 1–20.
45. Friedman, G.M. Distinction between dune, beach, and river sands from their textural characteristics. *J. Sediment. Res.* **1961**, *31*, 514–529. [CrossRef]
46. Folk, R.L.; Ward, W.C. Brazos River bar: A study of significance of grain size parameters. *J. Sediment. Petrol.* **1957**, *27*, 3–26. [CrossRef]
47. Blott, S.J.; Croft, D.J.; Pye, K.; Saye, S.E.; Wilson, H.E. Particle size analysis by laser diffraction. *Geol. Soc. Spec. Publ.* **2004**, *232*, 63–73. [CrossRef]
48. World Register of Marine Species (WORMS). Available online: https://www.marinespecies.org/ (accessed on 15 January 2026).
49. Fedra, K.; Feoli, E. GIS technology and spatial analysis in coastal zone management. *EEZ Technol.* **1998**, *3*, 171–179.
50. Clarke, K.R.; Warwick, R.M. *Change in Marine Communities: An Approach to Statistical Analysis and Interpretation*, 2nd ed.; PRIMER-E, Ltd., Plymouth Marine Laboratory: Plymouth, UK, 2001.
51. Sarconi, M. *Istoria de' Fenomeni del Tremuoto Avvenuto nelle Calabrie e nel Valdemone nell'Anno 1783, Posta in Luce dalla Reale Accademia delle Scienze e delle Belle Lettere di Napoli*; Campo, G., Ed.; Reale Accademia delle Scienze e delle Belle Lettere di Napoli: Napoli, Italy, 1784; pp. 1–197.
52. Vivenzio, G. *Historia dei Tremuoti Avvenuti nella Provincia di Calabria Ulteriore e nella Città di Messina Nell'Anno 1783 e di Quanto nelle Calabrie fu Fatto per Il Suo Risorgimento Fino al 1787, Preceduta da una Teoria, ed Istoria Generale de' Tremuoti*; Stamperia Regale: Napoli, Italy, 1788; Volume 2, pp. 1–441.
53. Maramai, A.; Graziani, L.; Brizuela Reyes, B. *Italian Tsunami Effects Database (ITED) (Version 1.0) [Data set]*; Istituto Nazionale di Geofisica e Vulcanologia (INGV): Rome, Italy, 2019. [CrossRef]
54. Guelorget, O.; Perthuisot, J.P. Le domaine paralique. Expressions géologiques, biologiques et économiques du confinement. In *Travaux du Laboratoire de Géologie de l'École Normale Supérieure*; Geology Laboratory of the École Normale Supérieure: Paris, France, 1983; Volume 16, pp. 1–136.
55. Zhang, C.; Yu, Z.; Zeng, G.; Jiang, M.; Yang, Z.; Cui, F.; Zhu, M.; Shen, L.; Hu, L. Effects of sediment geochemical properties on heavy metal bioavailability. *Environ. Int.* **2014**, *73*, 270–281. [CrossRef]

Disclaimer/Publisher's Note: The statements, opinions and data contained in all publications are solely those of the individual author(s) and contributor(s) and not of MDPI and/or the editor(s). MDPI and/or the editor(s) disclaim responsibility for any injury to people or property resulting from any ideas, methods, instructions or products referred to in the content.